JOURNAL OF MATERIALS SCIENCE 18 (1983) 2976–2986

Long-term ageing characteristics of Hastelloy alloy X

H. M. TAWANCY
Cabot Corporation, Kokomo, Indiana 46901, USA

Transmission electron microscopy and diffraction were used to characterize the microstructural changes which occur in Hastelloy* alloy X after long-term ageing (up to 16 000 h) at various temperatures in the range 540 to 870° C. The corresponding effects on mechanical properties were determined. It was found that the alloy age hardens at temperatures in the range of 650 to 870° C. Overageing occurred at 760 and 870° C. Marked reductions in room-temperature tensile elongation were observed after ageing at all the temperatures investigated. However, in no case was the elongation reduced to less than 15 to 30%. Also, the tensile elongation at temperatures corresponding to the respective ageing temperatures was unaffected by 16 000 h ageing at a temperature. It was concluded that the above effects were associated with precipitation of various phases, such as carbides, sigma- and mu-phases, in the matrix and at the grain boundaries.

1. Introduction

Hastelloy alloy X is a wrought, high-temperature, nickel-base superalloy that is commonly used in manufacturing combustor sections of jet engines, air craft tail pipes and furnaces. The alloy derives its strength from essentially solid solution. Table I shows its nominal chemical composition. The typical final heat treatment consists of annealing at 1175° C followed by rapid air cooling to produce an essentially single-phase material (f c c-solid solution). For many applications, it is important to characterize the microstructural changes which occur after long-term exposure to elevated temperatures and determine the corresponding effects on the mechanical properties. Previous work has shown that Hastelloy alloy X age hardens at 650 and 760° C [1]. Long-term exposure (up to 10 000 h) to these temperatures was found to cause substantial reductions in room-temperature impact toughness [1] and tensile elongation [2]. Based upon optical metallographic observations and X-ray diffraction measurements made on extracted phases, it was suggested that the observed degradation in mechanical strength was primarily due to precipitation of a carbide labelled at M_6C [1]. It is important to realize, however, that the inherent limitations of the above metallographic techniques can lead to inconclusive results concerning the metallurgical structure/property relationship of, particularly, multiphase complex superalloys [3]. In order to avoid those limitations, the technique of thin-foil transmission electron microscopy and diffraction was primarily employed for microstructural characterization in the present investigation.

2. Experimental procedure

The heat of the alloy investigated was of commercial grade and received in the form of 3.2 mm thick sheet that was annealed at 1175° C and then rapidly air cooled. Table I shows the chemical composition of the heat investigated. Metallographic and tensile test samples were aged for 100 to 16 000 h at 540, 650, 760 and 870° C and then air cooled. Property evaluation of aged material included measurements of room-temperature hardness and tensile properties and elevated temperature tensile properties at the respective ageing temperature after 16 000 h ageing at a temperature. Light optical metallographic samples were

*Hastelloy is a registered trademark of the Cabot Corporation.

0022–2461/83 $03.00 + .12

TABLE I Chemical composition (wt%)

	Ni	Cr	Fe	Mo	Co	Si	Mn	W	C
Nominal Composition of alloy X	Bal	22.0	18.5	9.0	1.50	1.0	1.0	0.60	0.10
Composition of the Heat Investigated	Bal	21.59	18.98	8.96	2.3	0.44	0.44	0.57	0.08

etched in a solution consisting of 80% concentrated HCl and 20% of 15 mol% chromic acid. Thin foils for transmission electron microscopy and diffraction work were prepared by the jet polishing technique in a solution consisting of 30 vol% nitric acid in methanol at about -20° C. All the foils were examined at an accelerating voltage of 100 kV.

3. Experimental results and discussion

3.1. Microstructural characterization in the annealed condition

Fig. 1 shows typical microstructures of the heat investigated in the annealed condition. The ASTM grain size number was predominantly 5. X-ray diffraction measurement of the lattice constant showed it to be 0.360 nm. It is typical of Hastelloy alloy X to contain a small amount of second-phase particles in the annealed condition, as shown in the example of Fig. 1a. This phase was identified by both X-ray and electron diffraction to be a molybdenum-rich carbide of the form M_6C (fcc with $a = 1.108$ nm). Usually, this carbide is referred to as "primary" in order to distinguish it from other carbide(s) which precipitate during ageing at elevated temperatures. On the finer scale of transmission electron microscopy, a relatively high dislocation density was observed at the carbide–matrix interface as shown in Fig. 1b. These dislocations could have formed during rapid cooling to accommodate the strain associated with the difference between the thermal expansion characteristics of the carbide and matrix. It will be shown later that these dislocations, as well as dislocations randomly dispersed throughout the matrix, have served as precipitation sites during ageing at elevated temperatures. Also, it will be shown that the molybdenum-rich, primary carbide has promoted the precipitation of molybdenum-rich phases such as the mu-phase.

3.2. Effect of ageing on room-temperature mechanical properties

Figs. 2 and 3 show, respectively, the effect of

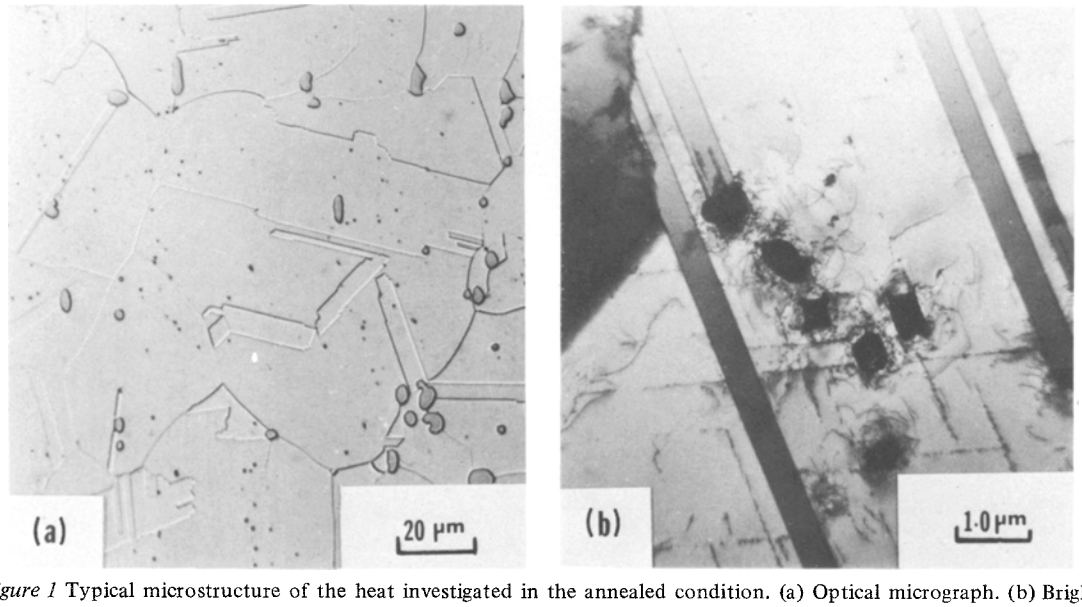

Figure 1 Typical microstructure of the heat investigated in the annealed condition. (a) Optical micrograph. (b) Bright field transmission electron micrograph.

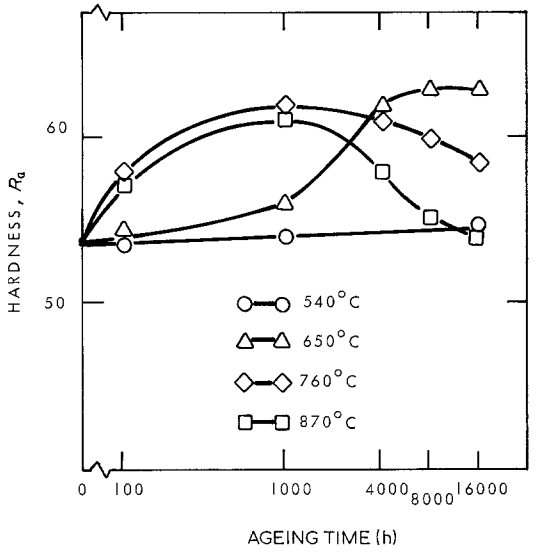

Figure 2 Effect of ageing time at the indicated temperatures on room-temperature hardness.

ageing time and temperature on hardness and tensile properties. This effect can be summarized as follows.

3.2.1. Ageing at 540° C

As can be seen from Figs. 2 and 3, ageing for up to 16 000 h had no significant effect on hardness and tensile strength. However, after 16 000 h it can be seen that the tensile elongation dropped by about 30%, relative to the annealed condition.

3.2.2. Ageing at 650° C

After 100 h of ageing, it can be seen that the tensile elongation dropped by about 20%. The hardness and tensile strength increased, but only slightly. No further significant change occurred up to 1000 h. A substantial increase in hardness, however, was observed after 4000 h of ageing. This was accompanied by marked strengthening and a substantial reduction in tensile elongation. For ageing times longer than 4000 h and up to 16 000 h, no further change took place.

3.2.3. Ageing at 760 and 870° C

The effect of ageing at 760 and 870° C was similar in that a substantial hardening accompanied by considerable reduction in tensile elongation

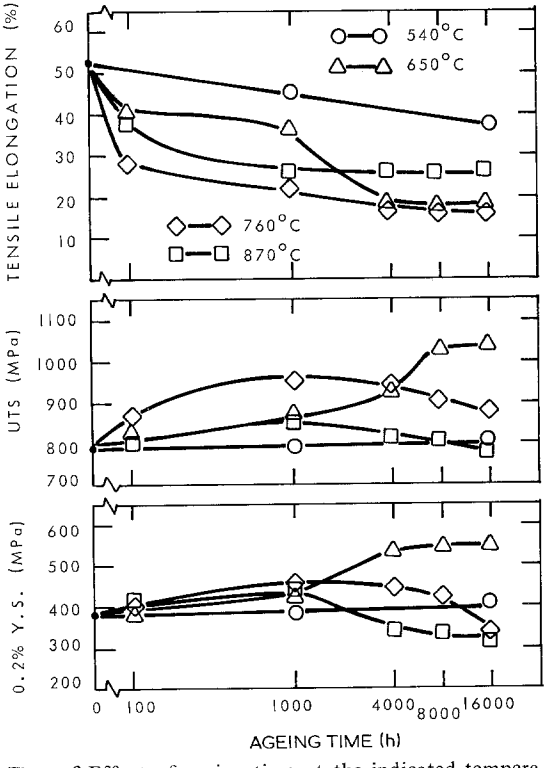

Figure 3 Effect of ageing time at the indicated temperatures on room-temperature tensile properties.

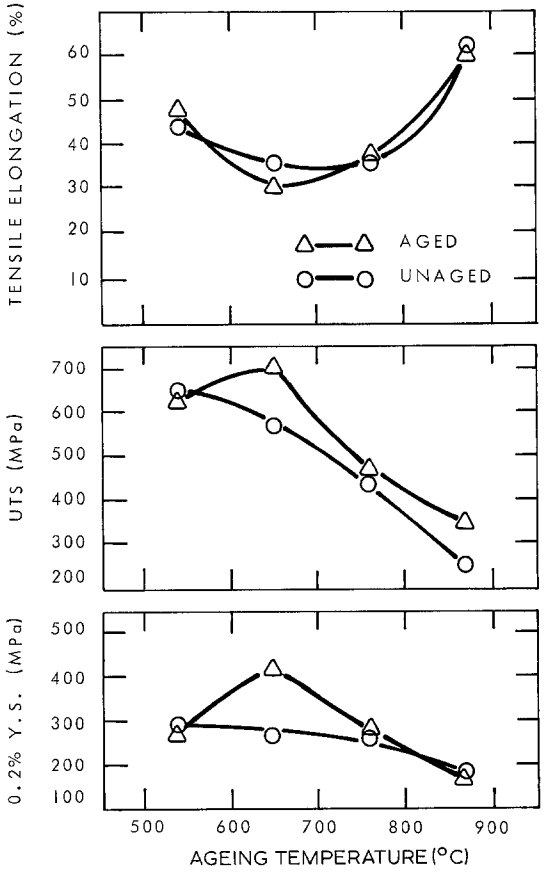

Figure 4 Elevated temperature tensile properties of unaged samples and samples previously aged 16 000 h at the respective test temperature.

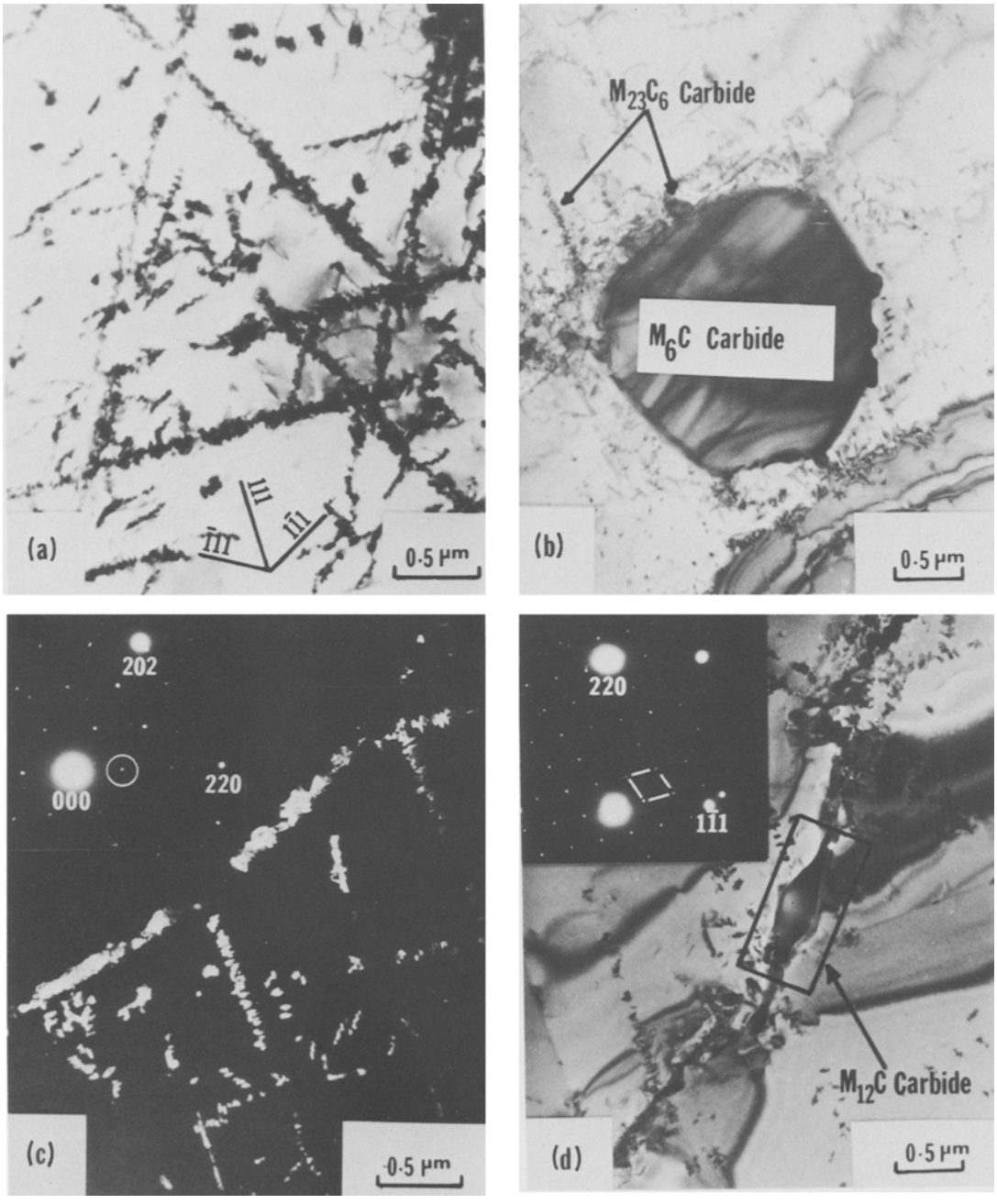

Figure 5 Electron micrographs showing characteristic microstructures after 16 000 h of ageing at 540° C.

occurred within the first 1000 of ageing, and overageing occurred after, at most, 4000 h of ageing at each temperature.

It could be concluded from the above observations that the heat investigated exhibited age hardening at 650, 760 and 870° C. However, various reductions in room-temperature tensile elongation occurred after ageing at all the temperatures investigated.

3.3. Effect of ageing on elevated temperature tensile properties

Fig. 4 shows elevated temperature tensile properties of unaged samples and samples aged 16 000 h at a temperature. All samples were tested at the respective ageing temperatures. Although ageing caused substantial reductions in room-temperature tensile elongation (Fig. 3), it can be seen from Fig. 4 that the tensile elongation at the respective

ageing temperature was almost unaffected by prior ageing. The room-temperature strengthening observed after ageing at 650° C was, however, maintained at 650° C. As discussed later, these effects could possibly be related to order–disorder transitions in sigma- and mu-phases.

3.4. Effect of ageing on microstructure

3.4.1. Ageing at 540° C

Optical metallography did not reveal marked microstructural changes after ageing for up to 16 000 h. On the finer scale of transmission electron microscopy, however, fine precipitates in the

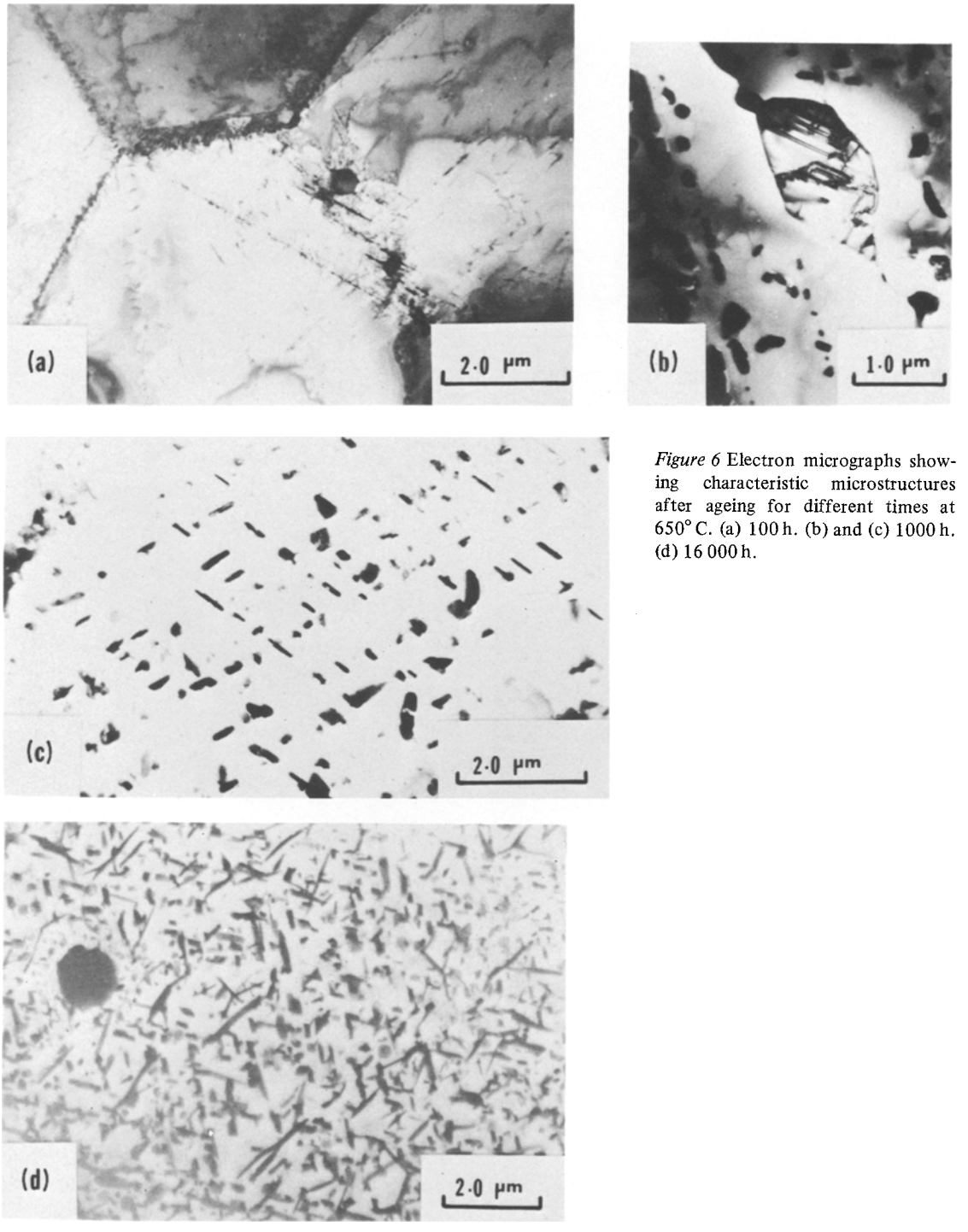

Figure 6 Electron micrographs showing characteristic microstructures after ageing for different times at 650° C. (a) 100 h. (b) and (c) 1000 h. (d) 16 000 h.

matrix and at the grain boundaries were observed. Fig. 5 exemplifies the characteristic microstructural features observed after 16 000 h of ageing. The matrix precipitates were primarily located at pre-existing matrix dislocations (Fig. 5a) and at the primary M_6C carbide–matrix interface (Fig. 5b). Electron diffraction showed that both the matrix precipitates and most of the grain boundary precipitates possessed the same crystal structure. Their characteristic reflections were present at every one-third position of the f c c matrix reflection (Fig. 5c). This observation indicated that those precipitates had a f c c structure with a lattice constant that was nearly three times that of the matrix; they also assumed the following orientation relationship with the matrix.

$$\{1\,0\,0\}_{\text{precipitate}} \parallel \{1\,0\,0\}_{\text{matrix}}$$

$$\langle 0\,0\,1\rangle_{\text{precipitate}} \parallel \langle 0\,0\,1\rangle_{\text{matrix}}$$

These are characteristic features of the chromium-rich $M_{23}C_6$ carbide (e.g. [4]). The dark field image of Fig. 5c, which was formed with a $M_{23}C_6$ carbide reflection of $1/3\,\langle 2\,2\,0\rangle$, indicated that both $M_{23}C_6$ carbides, in the matrix and at the grain boundaries, had assumed the same orientation. Another type of grain boundary precipitate having a f c c structure with a lattice constant of 1.089 nm was identified (Fig. 5d). This corresponds to a molybdenum-rich carbide of the form $M_{12}C$ [5–7]. The amount of this precipitate, however, was comparatively less than that of the $M_{23}C_6$ carbide at the grain boundaries. Generally, the amount of $M_{23}C_6$ carbides in the matrix was relatively small; however, the grain boundary carbides assumed a continuous layer which covered most of the boundaries. This could account for the observed reduction in room-temperature tensile elongation (Fig. 2).

3.4.2. Ageing at 650° C

After 100 h ageing, the microstructure was similar to that observed after 16 000 h at 540° C. That is, the matrix contained a relatively small amount of $M_{23}C_6$ carbides and a continuous carbide layer, consisting of mostly $M_{23}C_6$ carbides which were present at the grain boundaries (Fig. 6a). A phase with a characteristic internal structure was observed at the grain boundaries in addition to the $M_{23}C_6$

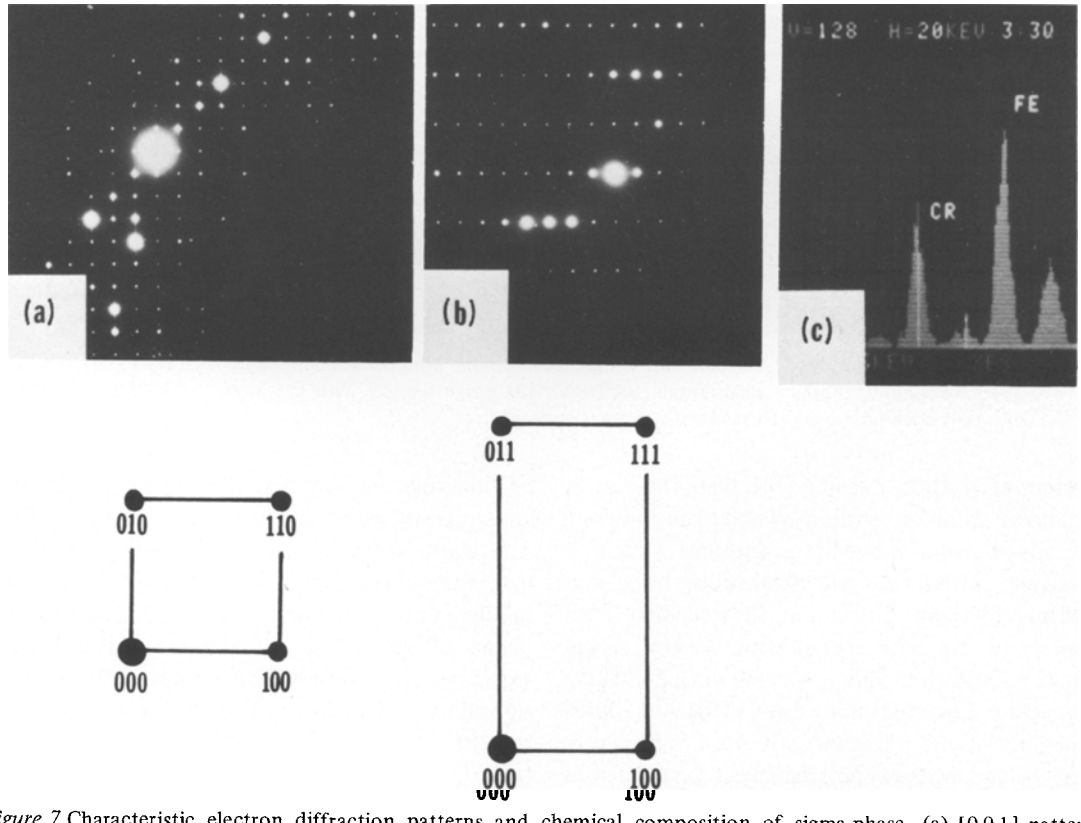

Figure 7 Characteristic electron diffraction patterns and chemical composition of sigma-phase. (a) [0 0 1] pattern. (b) [0 $\bar{1}$ 1] pattern. (c) X-ray spectrograph.

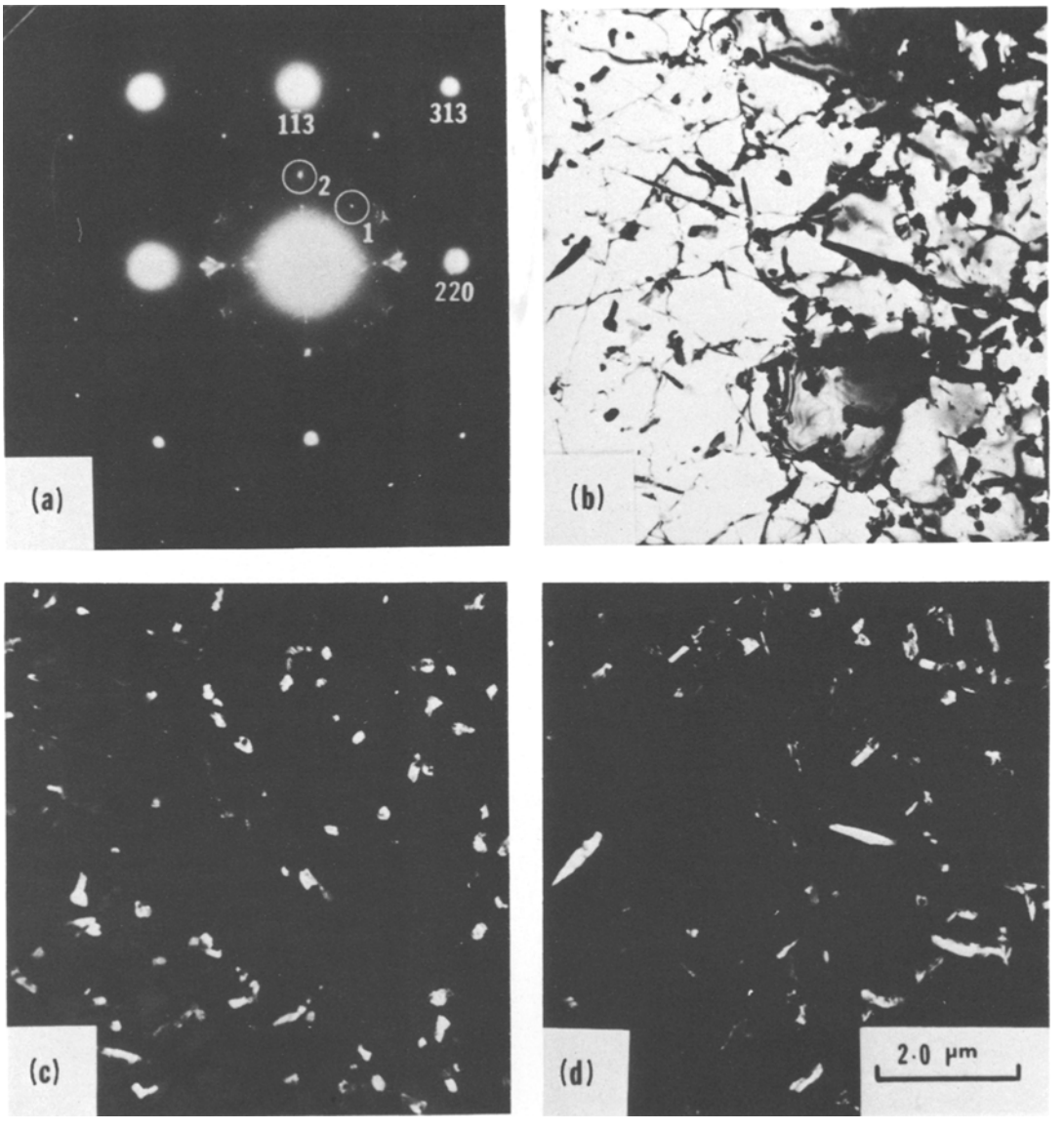

Figure 8 Distinction between $M_{23}C_6$ carbide and sigma-phase (sample aged for 4000 h at 650° C). (a) $[3\,\bar{3}\,2]_{fcc}$ matrix pattern. (b) Corresponding bright field image. (c) Dark field image formed with the $M_{23}C_6$ reflection 1 in (b) at $1/3\langle 3\,1\,3\rangle_{fcc}$. (d) Dark field image formed with sigma reflection 2.

carbides after 1000 h ageing (Fig. 6b). The matrix contained a phase with a platelet morphology intermixed with the $M_{23}C_6$ carbides (Fig. 6c). Striations within the platelets could be distinguished. Electron diffraction showed that both phases had the same crystal structure (tetragonal with $a = 0.880$ nm and $c = 0.454$ nm). Streaking was always observed along the [1 0 0] and [0 1 0] directions of the tetragonal structure as shown in Figs. 7a and b. X-ray microanalysis performed in the scanning transmission electron microscope on particles from that phase suspended from the edge of thin foils showed that the principal elemental constituents were chromium and iron (Fig. 7c). The above features correspond to a chromium–iron sigma-phase (e.g. [8]). Sequential faults were predicted to be present on the [1 0 0] and [0 1 0] planes of the tetragonal structure [9] and were experimentally observed in binary chromium–iron alloys [10]. This is further confirmed in the present investigation by the observed streaking (Fig. 7) and the characteristic internal structure (Fig. 6b). Fig. 8 shows an example of a dark field experiment used to distinguish the intermixed

$M_{23}C_6$ carbides and sigma-phase in the matrix. It is known that precipitation of sigma-phase is promoted by pre-precipitation of a phase enriched in a sigma-forming element (e.g. [8]). In the present case, pre-precipitation of the chromium-rich $M_{23}C_6$ carbides could have promoted the precipitation of sigma-phase. With continued ageing at 650° C, the density of the sigma-phase

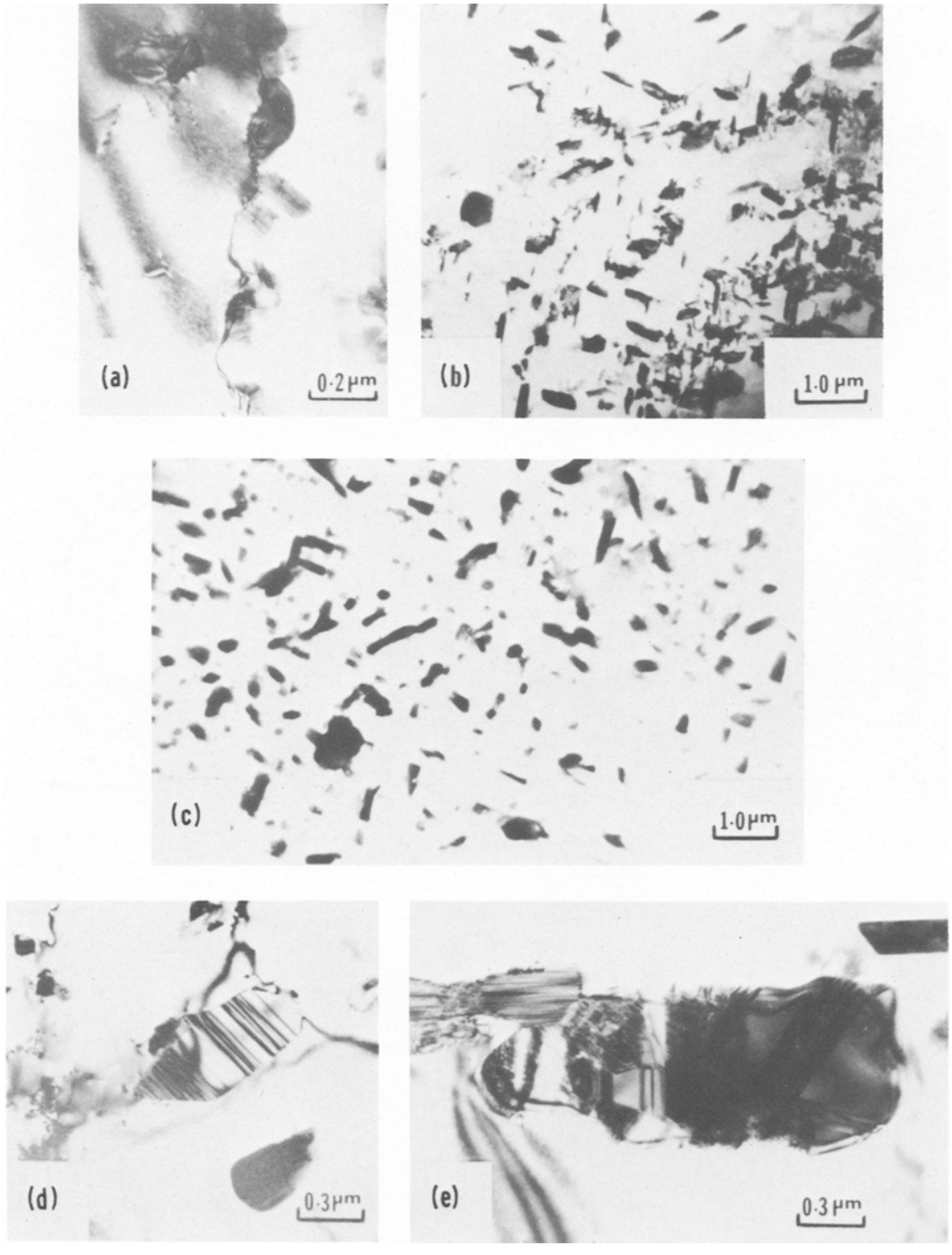

Figure 9 Electron micrographs showing characteristic microstructures after ageing for different times at 760° C. (a) 100 h, a mixture of sigma-phase and $M_{23}C_6$ carbides at a grain boundary. (b) 100 h, a mixture of sigma-phase and $M_{23}C_6$ carbides in the matrix. (c) 1000 h, a mixture of sigma-phase and $M_{23}C_6$ carbides in the matrix. Notice the increase in the density of the sigma-phase relative to (b). (d, e) 8000 h, blocky sigma-phase in the matrix.

continued to increase as can be seen by comparing Figs. 6c and d.

It could be concluded from the above results that the observed reduction in room-temperature tensile elongation in the early stages of ageing at 650° C was associated with precipitation of grain boundary carbides, mostly $M_{23}C_6$.

Sigma-phase, particularly in platelet morphology, is known to be extremely hard and brittle at room temperature [11]. Therefore, precipitation of sigma-phase in the later stages of ageing could cause the observed hardening, strengthening, and further reduction in room-temperature tensile elongation.

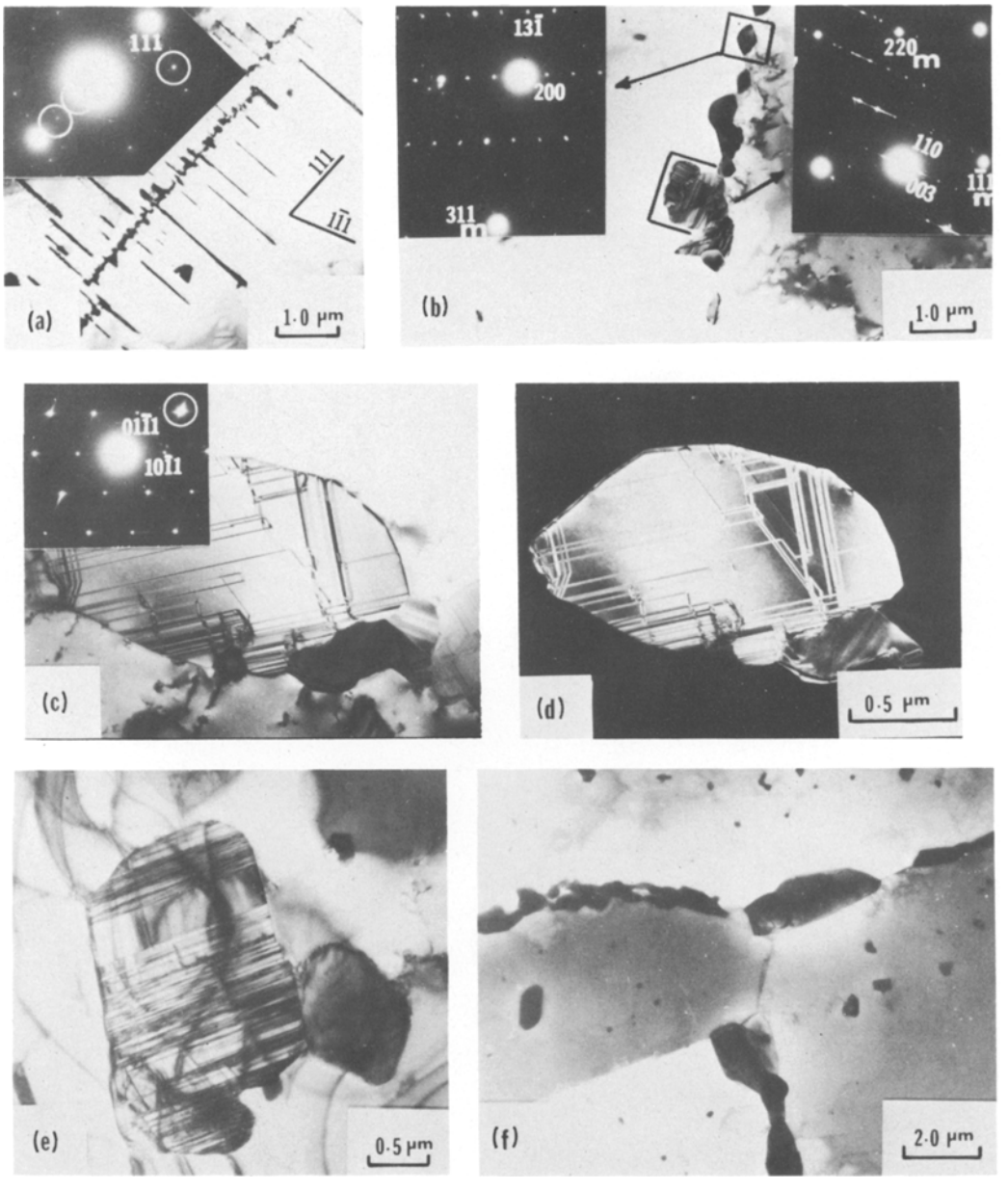

Figure 10 Electron micrographs showing characteristic microstructures after ageing for different times at 870° C. (a) 100 h, $M_{23}C_6$ carbides at the incoherent side of a twin boundary. (b) 100 h, a mixture of $M_{12}C$ carbides and mu-phase at a grain boundary. (c) 1000 h, bright-field image of a mu-phase particle in the matrix. (d) 1000 h, dark-field image of the mu-phase formed with the encircled reflection in (c). (d) 16 000 h, mu-phase particle in the matrix. (f) 16 000 h, $M_{12}C$ carbides at a grain boundary.

3.4.3. Ageing at 760° C

Fig. 9 shows characteristic microstructures after ageing for different times at 760° C. After 100 h ageing, sigma-phase precipitated at the grain boundaries and in the matrix in addition to the $M_{23}C_6$ carbides (Figs. 9a and b). Similar to the case at 650° C, the density of the sigma-phase continued to increase with progressive ageing as can be seen by comparing Figs. 9c and b. After 8000 h ageing, however, the sigma-phase had undergone considerable growth and had assumed a rather blocky-type of morphology (Figs. 9d and e). The observed hardening and reduction in room-temperature tensile elongation could then be associated, to a large extent, with the precipitation of sigma-phase. Growth of the sigma-phase in the later stages of ageing could account for the observed overageing.

3.4.4. Ageing at 870° C

After 100 h ageing, the precipitates formed were a $M_{23}C_6$ carbide, particularly at the incoherent sides of the twin boundaries (Fig. 10a), and a mixture of $M_{12}C$ carbides and a molybdenum-rich mu-phase at the grain boundaries (Fig. 10b). A small amount of mu-phase was also present in the matrix. The crystal structure of the mu-phase is hexagonal with $a = 0.476$ nm and $c = 0.257$ nm as calculated from electron diffraction patterns. With progressive ageing, the mu-phase continued to precipitate in the matrix and subsequently coarsened (Figs. 10c to e). Also, the density of the grain boundary precipitates increased. The mu-phase was characterized by its internal structure (Figs. 10b to e). Also, the mu-phase particles were almost always attached to the $M_{12}C$ carbide particles at the grain boundaries (Fig. 10b) and the

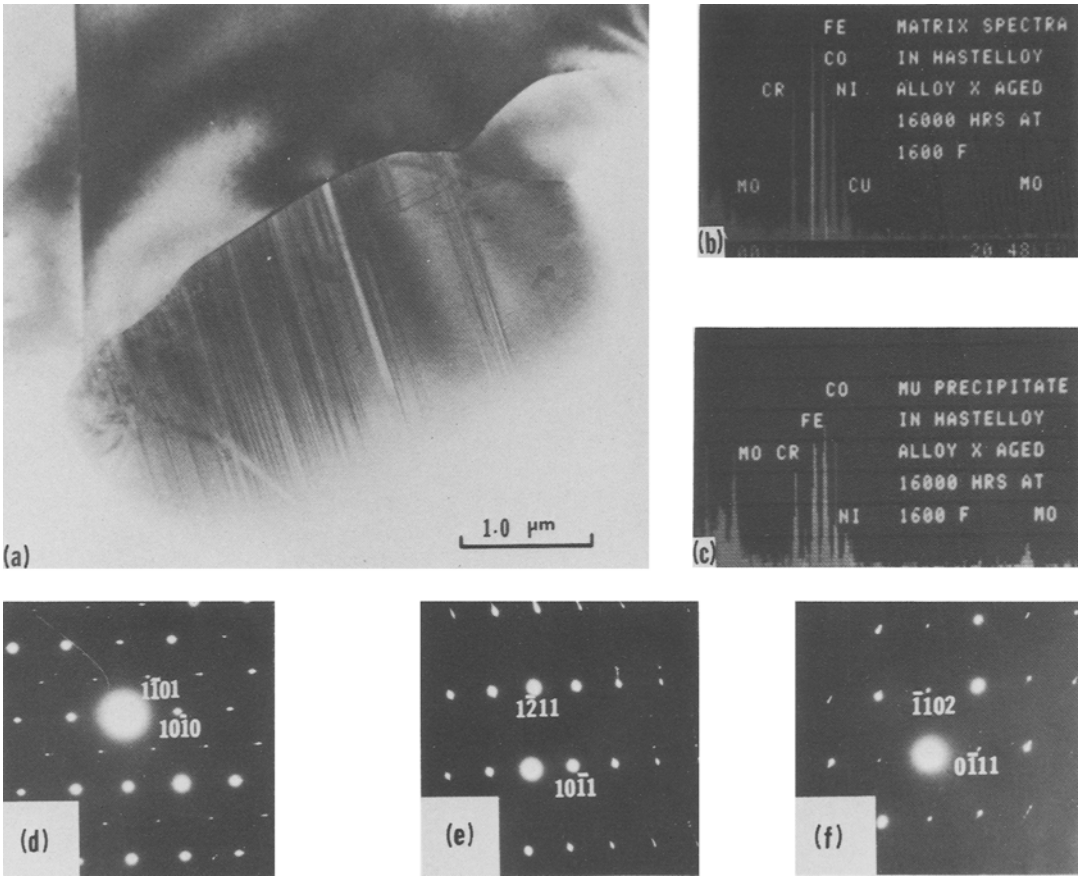

Figure 11 Characteristic electron diffraction patterns and chemical composition of mu-phase. (a) Bright field image. (b) X-ray spectrograph derived from the matrix in (a). (c) X-ray spectrograph derived from the mu-phase particle in (a). (d) [0 1 1] diffraction pattern derived from the mu-phase particle in (a). (e) $[\bar{1}\,0\,1]$ diffraction pattern derived from the mu-phase particle in (a). (f) $[\bar{1}\,1\,\bar{1}]$ diffraction pattern derived from the mu-phase particle in (a).

primary M_6C carbide particles (Figs. 10c and e). It is possible that the presence of the molybdenum-rich M_6C carbide and the pre-precipitation of the molybdenum-rich $M_{12}C$ carbide at the grain boundaries could have promoted the precipitation of the molybdenum-rich mu-phase. Fig. 10f is an example showing $M_{12}C$ carbides after 16 000 h ageing at 870° C. Fig. 11 shows an example of X-ray microanalysis performed in the scanning transmission electron microscope on a mu-phase particle suspended from the edge of a thin foil. It can be seen that the mu-phase is enriched in molybdenum as compared to the matrix. In indexing the diffraction patterns of the mu-phase in Figs. 9 and 10, it was not possible to check the absence of certain reflections because of the complexity of the crystal structure. However, it could be concluded from diffraction analysis that the internal structure of the mu-phase consisted of twin-related domains.

It is known that the mu-phase has a hardening and embrittling effect on nickel-based superalloys, particularly at room temperature [8]. Therefore, the observed hardening and reduction in room-temperature tensile elongation after ageing at 870° C could have been caused by precipitation of the mu-phase and also, to some extent, by precipitation of carbides. Coarsening of the mu-phase in the later stages of ageing could explain the observed overageing effect.

3.5. A remark on the effects of sigma- and mu-phases at elevated temperatures

Although sigma- and mu-phases are usually hard and brittle at room temperature, previous work has shown that they have ductile properties at elevated temperatures [8]. It was suggested that this is because of a lesser degree of order or an order–disorder transition in the sigma-phase [11] and a similar behaviour in the mu-phase [8]. This could provide a possible explanation for the observation that the embrittling effect of these phases at room temperature were absent at the respective ageing temperatures (Figs. 3 and 4).

4. Conclusions

The long-term ageing characteristics of Hastelloy alloy X in the temperature range of 540 to 870° C were studied. It could be concluded that:

1. The alloy age hardens at 650, 760 and 870° C primarily because of precipitation of the sigma-phase at 650 and 760° C and mu-phase at 870° C. Overageing occurs at 760 and 870° C because of coarsening of the sigma- and mu-phases, respectively, in the later stages of ageing.

2. The marked reductions in room-temperature tensile elongation are correlated with precipitation of carbides, mostly $M_{23}C_6$, at 540° C; sigma-phase and $M_{23}C_6$ carbides at 650 and 760° C; and mu-phase and $M_{23}C_6$ and $M_{12}C$ carbides at 870° C. However, in no case was the elongation reduced to less than 15 to 30%.

3. The detrimental effect of sigma- and mu-phases on room-temperature tensile elongation is absent at the respective ageing temperatures, possibly because of a lesser degree of order and/or order–disorder transitions in the sigma- and mu-phases.

Acknowledgements

It is a pleasure to acknowledge the assistance of Dr R. Gronsky of the Materials and Molecular Research Division of the Lawrence Berkeley Laboratory, University of California, Berkeley, in performing the scanning transmission electron microscopy experiments. Useful discussions with Dr G. Y. Lai are also acknowledged.

References

1. G. Y. LAI, *Met. Trans.* 9A (1978) 827.
2. S. J. MATTHEWS, in Proceedings of the 3rd International Conference on Superalloys, Seven Springs, September 1976, edited by B. H. Kear, D. R. Muzka, J. K. Tien and S. T. Wlodek (Claitor's Publishing Division, Baton Rouge, 1976) p. 215.
3. P. S. KOTVAL, *Metallography* 1 (1969) 251.
4. J. W. EDINGTON, "Typical Electron Microscope Investigations" (N. V. Philips, Gloeilampenfabrieken Eindhoren, 1976) p. 38.
5. H. M. TAWANCY, *J. Mater. Sci.* 16 (1981) 1117.
6. J. M. LEITNAKER, G. A. POTTER, D. J. BRADLY, J. C. FRANKLIN and W. R. LAING, *Met. Trans.* 9A (1978) 397.
7. A. C. FRACKER and H. H. STADELAMAIR, *Trans. AIME* 245 (1969) 857.
8. G. WALLWORK and J. CROLL, "Review of High-Temperature Materials", (Freund Publishing House, Ltd., Israel, 1976) p. 89.
9. F. C. FRANK and J. S. KASPER, *Acta Crystallogr.* 12 (1959) 483.
10. M. J. MARCINKOWSKI and D. S. MILLER, *Phil. Mag.* 7 (1962) 1025.
11. E. O. HALL and S. H. ALGIE, *Metall. Rev.* 11 (1966) 61.

Received 25 November 1982
and accepted 18 February 1983